EC
Journals.ASM.org

The Plasma Membrane Proton Pump PMA-1 Is Incorporated into Distal Parts of the Hyphae Independently of the Spitzenkörper in *Neurospora crassa*

Rosa A. Fajardo-Somera,[a] Barry Bowman,[b] Meritxell Riquelme[a]

Department of Microbiology, Center for Scientific Research and Higher Education of Ensenada (CICESE), Ensenada, Baja California, Mexico[a]; Department of Molecular, Cell & Developmental Biology, University of California, Santa Cruz, California, USA[b]

Most models for fungal growth have proposed a directional traffic of secretory vesicles to the hyphal apex, where they temporarily aggregate at the Spitzenkörper before they fuse with the plasma membrane (PM). The PM H^+-translocating ATPase (PMA-1) is delivered via the classical secretory pathway (endoplasmic reticulum [ER] to Golgi) to the cell surface, where it pumps H^+ out of the cell, generating a large electrochemical gradient that supplies energy to H^+-coupled nutrient uptake systems. To characterize the traffic and delivery of PMA-1 during hyphal elongation, we have analyzed by laser scanning confocal microscopy (LSCM) strains of *Neurospora crassa* expressing green fluorescent protein (GFP)-tagged versions of the protein. In conidia, PMA-1-GFP was evenly distributed at the PM. During germination and germ tube elongation, PMA-1-GFP was found all around the conidial PM and extended to the germ tube PM, but fluorescence was less intense or almost absent at the tip. Together, the data indicate that the electrochemical gradient driving apical nutrient uptake is generated from early developmental stages. In mature hyphae, PMA-1-GFP localized at the PM at distal regions (>120 μm) and in completely developed septa, but not at the tip, indicative of a distinct secretory route independent of the Spitzenkörper occurring behind the apex.

One of the main features of filamentous fungi is their apical mode of growth. In filamentous fungi, cell wall growth and exocytosis are linked processes that involve the highly polarized traffic of cell wall-building secretory vesicles to apical areas, where they deliver proteins and lipids. One of the most widely accepted models for fungal growth, the vesicle supply center for fungal morphogenesis, postulates a unidirectional traffic of vesicles to the hyphal apex, where they aggregate temporarily at an apical structure, the Spitzenkörper, prior to fusion with the apical plasma membrane (PM) by the process of exocytosis (1). However, some PM proteins, such as the H^+-ATPases, essential for hyphal growth, have been previously predicted to be absent or inactive at the hyphal apex (2–4), suggesting the existence of vesicle delivery routes other than the above and independent of the Spitzenkörper that reach nonapical regions of the hyphal PM. H^+-ATPases are involved in pumping protons out of the cell, generating a large electrochemical gradient and supplying energy to H^+-coupled nutrient uptake systems (5). This electrochemical gradient has been studied in several fungal species by diverse methods, including vibrating probes, microelectrodes, and pH indicators. The results showed that current normally flows inward at the hyphal apical regions and flows outward at distal areas (3, 4, 6–9).

PMA1, the H^+-ATPase-encoding gene in *Saccharomyces cerevisiae* (SCRG_01016 [10]), has a single homolog in *Neurospora crassa* (NCU01680 [11, 12]). In *S. cerevisiae*, Pma1p is one of the most abundant proteins of the cell surface (25 to 50%), while in *N. crassa*, it constitutes about 5 to 10% of the PM total protein content (13, 14).

In *S. cerevisiae*, Pma1p is delivered to the cell surface via the classical endoplasmic reticulum (ER) to the Golgi secretory pathway defined by the *SEC* genes (15–17), where specialized proteins ensure the efficient transport of Pma1p through the secretory pathway. For instance, Lst1p (Sec24p homolog) is involved in the export of Pma1p from the ER. Together with Sec23p, Lst1p is necessary for the efficient packing of Pma1p into ER-derived COPII vesicles (18, 19). Furthermore, Ast1p and Ast2p participate in the transport of Pma1p from Golgi to the PM (20). Upon arrival to the PM, Pma1p is very stable (with a half-life of >12 h [21]). Lipid rafts have a role in sorting Pma1p to the PM. Upon lipid raft disruption, Pma1p is missorted to the vacuole, where it is degraded (22). In Δ*elo3* and Δ*lcb1* mutants, defective in lipid rafts, mutant *pma1-7* is not degraded in vacuoles. Instead, it is delivered to the PM (23, 24).

As part of an ongoing project to characterize the relationship between the secretory pathway and hyphal growth in filamentous fungi, we have analyzed the biogenesis and trafficking of the PM H^+-translocating ATPase in *N. crassa* by fusing the gene *pma-1* to *gfp* and studying the location of PMA-1 in living cells during vegetative development.

MATERIALS AND METHODS

Culture conditions. *N. crassa* cells were grown on Vogel's minimal medium agar (VMM [25]) supplemented with histidine (0.1 mg/ml) when needed. Liquid cultures were grown in Vogel's complete medium (VCM; 1× Vogel's salts, 1.5% sucrose, 0.5% yeast extract, 0.5% Casamino Acids) at 30°C and 200 rpm for 16 h. For transformation, conidia were spread directly on plates containing FGS medium (0.05% fructose, 0.05% glucose, 2% sorbose) or mixed with top agar (1× Vogel's salts, 1 M sorbitol,

Received 28 January 2013 Accepted 28 May 2013
Published ahead of print 31 May 2013
Address correspondence to Meritxell Riquelme, riquelme@cicese.mx.
Supplemental material for this article may be found at http://dx.doi.org/10.1128/EC.00328-12.

doi:10.1128/EC.00328-12

TABLE 1 Plasmids and strains used or generated in this study

Plasmid or strain	Characteristics or genotype	Reference or source
Plasmids		
pMF272	P*ccg-1*::*sgfp*$^+$	29
pZERO-GFP	P*ccg-1*::*10Xgly*::*gfp*$^+$::*loxp*$^+$::*hph*$^+$::*loxp*$^+$	30
pMR001	P*ccg-1*:: *pma-1*::*sgfp*$^+$	This study
Strains		
N1	*mat***a**	FGSC#988
N150	*matA*	FGSC#9013
SMRP277	*mat***a** *sad-2*Δ::*hph*$^+$	FGSC#20680
SMRP278	*matA sad-2*Δ::*hph*$^+$	32
N39	*matA fl*	FGSC#4317
N40	*mat***a** *fl*	FGSC#4347
VMA-1-RFP	*matA vma-1-rfp*$^+$	FGSC#10169
SMRP24	*matA his-3 mus-51*Δ::*bar*$^+$	FGSC#9717
SMRP25	*mat***a** *mus-51*Δ::*bar*$^+$	FGSC#9718
TESM001-3[a]	*matA his-3*$^+$::P*ccg-1*::*pma-1*::*sgfp*$^+$	This study
TRAF6-5[a]	*mat***a** native promoter *pma-1*::*sgfp*$^+$	This study
TRAF9-1[a]	*mat***a** native promoter *pmb*::*sgfp*$^+$	This study
NRAF6-11	*mat***a** native promoter *pma-1*::*sgfp*$^+$	This study
NRAF9-1	*mat***a** native promoter *pmb*::*sgfp*$^+$	This study

[a] Heterokaryon.

1% agar, 1× FGS) and spread onto 3 petri dishes containing FGS medium supplemented with hygromycin (300 μg/ml).

For confocal microscopy, transformants of *N. crassa* expressing green fluorescent protein (GFP) and/or red fluorescent protein (RFP) were routinely grown on VMM overnight at 30°C. For imaging, the inverted agar block method was used as previously described (27). Strains used or generated in this study are listed in Table 1.

Recombinant DNA techniques and plasmid constructions. Since *pma-1* is an essential gene, PMA-1-GFP, under the control of the *ccg-1* promoter, was targeted to the *his-3* locus. Standard methods were used for cloning procedures to fuse GFP to the carboxy terminus of PMA-1 (28). PCR was performed in a Bio-Rad thermal cycler using Platinum *Pfu* polymerase (Invitrogen) according to the manufacturer's instructions. The predicted *pma-1* gene (3,077 bp; NCU01680.4) was amplified from *N. crassa* genomic DNA by PCR using custom-designed primers. Forward primer PMA-1-XbaI-F at the 5′ end of the gene contained an introduced XbaI restriction site; reverse primer PMA-1-PacI-R at the 3′ end of the gene sequence, excluding the stop codon, contained a PacI restriction site (Table 2). The amplified and purified PCR product was digested with XbaI and PacI and cloned into XbaI- and PacI-digested plasmid pMF272 (NCBI GenBank accession number AY598428 [29]), yielding plasmid pMR001. All plasmids were propagated in *Escherichia coli* strain DH5α supercompetent cells (Invitrogen). Sequencing of plasmid pMR001 was carried out at the Core Instrumentation Facility of the Institute for Integrative Genome Biology at the University of California, Riverside.

To overcome potential mislocalization of GFP-tagged PMA-1 due to overexpression driven by the *ccg-1* promoter, we constructed a strain in which the 3′ end of the endogenous *pma-1* was fused to the *gfp* gene, using fusion PCR (see Fig. S1 in the supplemental material) (M. Riquelme, E. L. Bredeweg, O. Callejas-Negrete, R. W. Roberson, S. Ludwig, A. Beltrán-Aguilar, S. Seiler, and M. Freitag, unpublished data). Primer pairs ORFS54-F P1–ORFS55-R P2 and ORFS56-F P3–ORFS57-R P4 (Table 2) were used to amplify 1 kb of the *pma-1* open reading frame (ORF) and 3′ untranslated region (UTR), respectively, from *N. crassa* genomic DNA. The cassette *gfp-hph* was amplified using primers 10XGlyF P7 and loxPR P8 (Table 2) from plasmid pCCG-1::Gly::GFP (30). Both fragments (ORF or 3′ UTR) and the cassette *gfp-hph* were fused by PCR using primers pairs ORFS54-F P1–hph SMR P6 (Table 2) to amplify 1 kb of the ORF fused to *gfp-hph* and hph SMF P5–ORFS57-R P4 (Table 2) to amplify *hph* fused to 1 kb of the 3′ UTR. PCRs were performed in a Lab Line thermal cycler

TABLE 2 Oligonucleotides used or generated in this study

Oligonucleotide	Sequence	Source or reference
PMA-1-Xba-F	5′- AATCTAGACGCCAATGGCGGACCACTC-3′	This study
PMA-1-PacI-R	5′-CGTTAATTAATTGCGACTTCTCATGCTGAG-3′	This study
ORFS45-F P1	5′-CGAGCCGGGTGCTTTTGCTCCCTA-3′	This study
ORFS46-R P2	5′-TCCGCCTCCGCCTCCGCCGCCTCCGCCACCCATGATACCCGTTCC-3′	This study
ORFS47-F P3	5′-TATACGAAGTTATGGATCCGAGCTCGGGGGATGGTATAATGGAAGG-3′	This study
ORFS48-R P4	5′-CGCTTTCCGTCCTTCTGCAACCAC-3′	This study
ORFS54-F P1	5′-GCCCGGCTCTGAGGTCTACGAC-3′	This study
ORFS55-R P2	5′-CCGCCTCCGCCTCCGCCGCCTCCGCCTTGCGACTTCTCATGCTGAG-3′	This study
ORFS56-F P3	5′-GCTATACGAAGTTATGGATCCGAGCTCGGCGATATAATGATTTTCC-3′	This study
ORFS57-R P4	5′-CCACAAACCAGAAATAACCGTGCC-3′	This study
ORFS87-F P1seq	5′-CCTCCCCGTCACGATACCTAC-3′	This study
ORFS88-F P2seq	5′-CCGTATCTGGATCTTCTCCTTC-3′	This study
ORFS89-F P1seq	5′-GTCATTTTCGTCATCAACCTG-3′	This study
ORFS90-F P2seq	5′-CAAGGCTTCACCGCGTTCATGC-3′	This study
hph SMR P6	5′-TCGCCTCGCTCCAGTCAATGACC-3′	Riquelme et al., unpublished
hph SMF P5	5′-AAAAAGCCTGAACTCACCGCGACG-3′	Riquelme et al., unpublished
10XGlyF P7	5′-GGCGGAGGCGGCGGAGGCGGAGGCGGAGG-3′	Riquelme et al., unpublished
loxPR P8	5′-CGAGCTCGGATCCATAACTTCGTATAGCA-3′	Riquelme et al., unpublished
OMF1651-R	5′-CGGCTGAAGCACTGCACGCCG-3′	Freitag lab
MRp10 F	5′-AGAGACAAGAAAATTACCCCCTTCTT-3′	31
MRp11 R	5′-AACTACAACAGCCACAACGTCTATATC-3′	31
MRp12 F	5′-ATAATGAACGGAAGGTAGTTGTAGAAAG-3′	31
MRp13 R	5′-ATGGATATAATGTGGCTGTTGAAAG-3′	31
pMF272F	5′-CAAATCAACACAACACTCAAACCA-3′	31
pMF272 R	5′-GGCACCACCCCGGTGAACAGCTCC-3′	31

using TaKaRa DNA polymerase (TaKaRa Inc.). *pmb*, the basic amino acid permease-encoding gene (NCU05168.4), was *gfp* tagged using the same strategy with primer pairs ORFS45-F P1 and ORFS46-R P2 and ORFS47-F P3 and ORFS48-R P4.

***Neurospora* genetic methods.** Transformation of *N. crassa* strain FGSC#9717 conidia (*his-3*; Δ*mus-51 matA*) with plasmid pMR001 (DraI linearized) was carried out by electroporation on a Bio-Rad Gene Pulser (25-μF capacitance, 1.5-kV voltage, and 600-Ω resistance). *his-3*$^+$ prototrophic transformants showing fluorescence were selected (TESM003). The correct integration of the recombinant cassette in the selected transformant, TESM001-3, was verified by PCR using primers MRp10 F, MRp11 R, MRp12 F, and MRp13 R as previously reported (31).

For transformation with DNA fragments obtained from fusion PCR, conidia of *N. crassa* strain FGSC#9718 (Δ*mus-51 mat***a**) were used. Hygromycin (300 μg/ml)-resistant heterokaryon transformants (PMA-1-GFP or PMB-GFP) showing fluorescence were selected (TRAF6-5 and TRAF9-1, respectively).

To obtain homokaryon strains expressing PMA-1-GFP or PMB-GFP, we crossed *N. crassa* heterokaryon strains TRAF6-5 and TRAF9-1 with *N. crassa* Δ*sad-2* (*matA* [32]). Hygromycin (300 μg/ml)-resistant colonies that showed fluorescence were selected (NRAF6-11 and NRAF9-1).

Correct integration in NRAF6-11 and NRAF9-1 strains was verified by PCR using primer pairs ORFS87-F P1 seq/OMF1651-R and ORFS88-F P2 seq/hph SMR P6 and primer pairs ORFS89-F P1 seq/OMF1651-R and ORFS90-F P2 seq/hph SMR P6, respectively (see Fig. S2 in the supplemental material). Mycelium for genomic DNA extraction was grown at 28°C for 7 days on liquid medium with no shaking and no light, filtered, submerged in liquid nitrogen, and lyophilized. DNA was extracted with the DNeasy plant extraction kit (Qiagen).

Sucrose gradient and Western blot analysis. Liquid Vogel's complete medium (VCM) was inoculated with NRAF6-11 (1×10^6 conidia/ml) and incubated for 16 h at 30°C and 200 rpm. Mycelia were filtered by vacuum, triturated with liquid nitrogen, and homogenized with 1 volume of glass beads (0.5 mm; Sigma) and 2 volumes of 33 mM phosphate buffer pH 8.2 (38) in a Braun MSK homogenizer for 4 pulses for 30 s each time in the presence of CO_2 flow as the coolant. The homogenate was centrifuged at 5,000 × *g* for 5 min at 4°C. The total extract was loaded onto a sucrose gradient as described previously (33). Density (Abbe refractometer; Carl Zeiss, Göttingen, Germany) and absorbance (280 nm, 6505 UV-visible [UV-Vis] spectrophotometer; Jenway) were determined for each fraction.

For Western blot analysis, 30 μl of each fraction was loaded per lane. The samples were heated at 37°C for 30 min and run in a 7% SDS-polyacrylamide gel. Anti-GFP (1:500; Santa Cruz Biotechnology) and goat anti-mouse IgG conjugated to horseradish peroxidase (1:1000; Roche) were used as primary and secondary antibodies, respectively.

Fluorescence microscopy and image processing. Cells expressing GFP were imaged using an inverted Zeiss laser scanning confocal microscope (LSM-510; Carl Zeiss) and an Olympus FluoView FV1000 confocal microscope (Olympus, Japan), both fitted with an argon ion laser with a GFP filter set with a 488-nm excitation wavelength and a 505- to 550-nm emission wavelength and an He/Ne1 laser with an RFP filter set with a 543-nm excitation wavelength and a 560-nm emission wavelength. A 100× (PH3), 1.3-numerical aperture (NA) Plan-Neofluar oil immersion objective was used for LSM-510. For FV1000, a 60×, 1.42-NA Plan-Apochromat oil immersion objective was used. A photomultiplier module allowed us to combine the confocal with phase-contrast or differential interference contrast (DIC) to provide us with a simultaneous view of the fluorescently labeled proteins and the entire cell. The imaging parameters used produced no detectable background signal from any source other than from GFP. Time-lapse imaging was performed at scan intervals of 1.5 to 30 s for periods up to 40 min and captured with a combination of low energy, high attenuation, and a less concentrated excitation laser beam caused by the low-NA objective, to avoid photobleaching during repetitive imaging. Confocal images were captured using LSM-510 (version 3.2; Carl Zeiss) or Olympus Fluoview (version 4.0a; Olympus) software and evaluated with an LSM-510 image examiner (version 3.2) or Olympus Fluoview viewer (version 4.0a), respectively. Some of the time series were converted into animation movies using the same software.

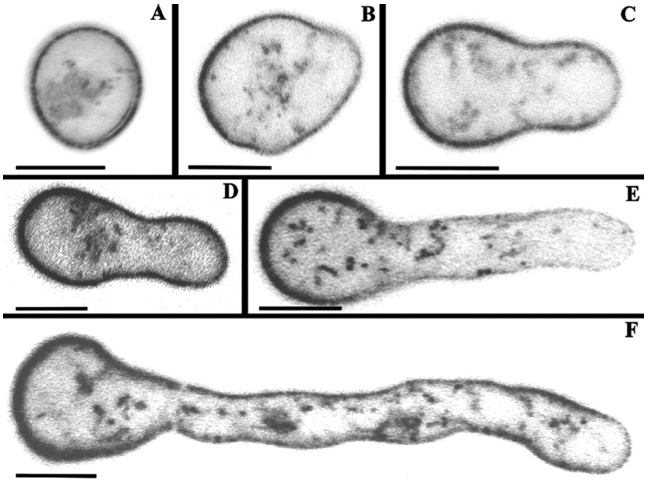

FIG 1 PMA-1-GFP expression under the control of the *pma-1* native promoter in conidia and germlings of *N. crassa*. (A) In conidia, PMA-1-GFP was evenly distributed along the PM; (B to F) in young germlings, ranging from 7 to 49 μm in length, PMA-1-GFP accumulated all along the PM, although with less intensity at the apex. Bars = 5 μm.

To analyze the distribution of the PMA-1-GFP fluorescence, a reconstruction was made with Adobe Photoshop CS5 for 20 hyphae, taking 10 frames for each hypha along its longitudinal axis. The first captured frame included the hyphal apex up to the region starting to show fluorescence; the next 9 frames included the region behind the first frame to the region where fluorescence could be observed in the PM. After incubation for 5 h, germinated conidia of strains expressing PMA-1-GFP (under the control of native or *ccg-1* promoters) were imaged and the fluorescence of the PMA-1–GFP driven by P*ccg-1* was measured from the base of the conidium to the region of the germ tube PM where fluorescence was no longer observed.

For fluorescence recovery after photobleaching (FRAP) analysis, a region of interest was selected, and 500 repetitions at 90% laser intensity were applied during a time series sequence acquisition. Triplicate experiments were performed. For fluorescence intensity measurements before and after photobleaching, ImageJ (National Institutes of Health, USA) software was used. FRAPAnalyser (University of Luxembourg) was used to obtain fluorescence recovery plots and fitted curves. All analyses were submitted to a background subtraction. Nonadjacent unbleached PM regions were used as reference controls.

Cells stained with FM4-64 [*N*-(3-triethylammoniumpropyl)-4-(6-(4(diethylamino) phenyl) hexatrienyl) pyridinium dibromide; Molecular Probes] were imaged with the argon ion laser (excitation wavelength, 514 nm, and emission wavelength, 670 nm).

For each treatment, agar blocks containing hyphae were inverted onto a coverslip containing a 10-μl drop of the corresponding solution. Cells were imaged 5 to 10 min after that.

Inhibitors and fluorescent dyes. An inhibitor of the classical ER-Golgi secretory pathway, brefeldin A (BFA; Sigma), was added to growing hyphae at a final concentration of 200 μg/ml in VMM from a 20-mg/ml stock solution in dimethyl sulfoxide (DMSO). FM4-64 was used at a final concentration of 10 μM in VMM. Cytoskeleton inhibitors were used to disturb the Spitzenkörper. Stock solutions of cytochalasin A (Sigma; 1 mg/ml) and latrunculin A (Sigma; 400 μg/ml), both actin inhibitors, were prepared in DMSO and diluted in VMM to working concentrations of 50 μg/ml and 20 μg/ml, respectively. A stock solution of methyl 1-(butylcarbamoyl)-2-benzimidazolecarbamate (benomyl; Sig-

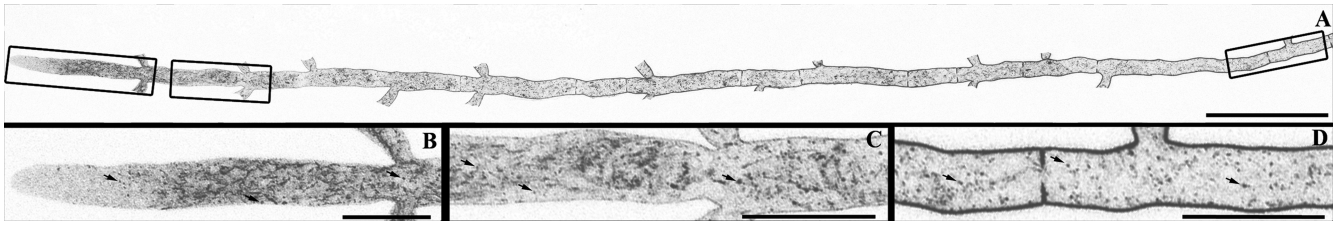

FIG 2 Distribution of PMA-1-GFP in a mature hypha of *N. crassa*. (A) Reconstruction of a growing hypha imaged by LSCM; (B to D) magnifications of boxes in panel A. (B) At the hyphal subapex (>50 μm from the tip), PMA-1-GFP localized at individual vesicles (arrows); (C) behind the subapex, PMA-1-GFP localized at the tubular endomembrane system; (D) in distal areas (>120 μm under the native promoter), PMA-1-GFP localized at the PM of septa. Bars = 50 μm (A) and 20 μm (B to D).

ma; 500 μg/ml), a microtubule inhibitor, was prepared in ethanol and diluted in VMM to a working concentration of 100 μg/ml.

RESULTS

Selection of strains expressing PMA-1-GFP. Strains showing fluorescence were selected by screening prototrophic transformants by laser scanning confocal microscopy (LSCM). The integration of the *pma-1-gfp* cassette at the *his-3* locus was confirmed by PCR, yielding the predicted 3.2-kb amplicon with primers MRp10 F and MRp11 R and a 2.1-kb amplicon with primers MRp12 F and MRp13 R (data not shown). The correct integration of the *pma-1-gfp-hph* and *pmb-gfp-hph* cassettes was confirmed by PCR with primers sets ORFS87-F P1seq–OMF1651-R and ORFS88-F P2seq–OMF1651-R to *pma-1* and with primers sets ORFS89-F P1seq–OMF1651-R and ORFS90-F P2seq–OMF1651-R to *pmb*, obtaining the expected 1.5-kb and 2.1-kb amplicons (data not shown). Strains TESM003, NRAF6-11, and NRAF9-1 showing stable fluorescence were selected for subsequent analyses.

Although the strain expressing PMA-GFP under the control of the endogenous promoter grew slower than the corresponding parental strain (see Fig. S3 in the supplemental material), it showed wild-type hyphal morphology. *pma-1* is an essential gene; therefore, the viability of the strain with the replacement of the native gene with a *pma-1-gfp* version indicated that the recombinant protein was functional. Therefore, all subsequent microscopy analyses were conducted using the strain in which PMA-1-GFP was expressed under the control of the native promoter.

The molecular mass of *N. crassa* PMA-1 is 99.88 kDa (920 amino acids), but when the protein is tagged with GFP, the molecular mass increases to 126.8 kDa, as confirmed by Western blotting (see Fig. S4B in the supplemental material). We used a sucrose gradient to identify PMA-1-GFP-containing vesicles according to their buoyant densities and to compare the buoyant densities with those of previously reported markers of the secretory pathway. PMA-1-GFP was detected in fractions 7 to 19, corresponding to densities ranging between 1.103 and 1.213 g/ml. The strongest signal was observed for high-density fractions 15 and 16 (see Fig. S4A and B), corresponding to 1.155 and 1.158 g/ml. This indicated that PMA-1 travels in high-density vesicles and is found at the PM (34, 35).

PMA-1-GFP is absent in the apical plasma membrane. PMA-1-GFP was practically absent at the apex of the PM of germlings. The distribution of PMA-1-GFP was analyzed during the different germination phases, previously established (36, 37): phase I, conidia during hydration; phase II, germ tube emergence; phase III, germ tube elongation, and phase IV, mature hyphae. In nongerminated conidia growing isotropically during phase I, PMA-1-GFP fluorescence was evenly distributed throughout the PM (Fig. 1A). In the next phases of germination (II and III), expression of PMA-1-GFP was found all around the conidial PM and extended to the germ tube PM, although at the tip the fluorescence was less intense or almost absent (Fig. 1B to F).

In mature hyphae, PMA-1-GFP was localized at the PM at distal hyphal regions and in already completed septa. Mature hyphae are subdivided in three regions: region I, or hyphal apex (the first 1 to 5 μm); region II, or subapical region (5 to 20 μm); and region III, or distal region (>20 μm) (36). In mature hyphae, PMA-1-GFP was found in the PM at far distal regions (>120 μm from the apex) (Fig. 2A). PMA-1-GFP did not accumulate at the PM in hyphal region I or II or the first portion of region III (Fig. 2A and B). In distal region III, PMA-1-GFP could be found in the lumen of tubular endomembranes (Fig. 2B). These tubular endomembranes partially colocalized with the vacuolar H^+-translocating ATPase VMA-1 (Fig. 3). In distal regions, we observed PMA-1-GFP in the lumen of globular vacuoles, whereas VMA-1-RFP was found at the membrane of the globular vacuoles (Fig. 3A to D). Furthermore, we observed small vesicular carriers in germlings and in apical and distal regions of hyphae (Fig. 1 and 2). These small vesicles seemed to fuse with the PM, and they did not colocalize with FM4-64 (see Movies S1 and S2 in the supplemental material).

In distal regions, PMA-1-GFP was also found in the PM of mature septa (Fig. 2D, 3, and 4J). To investigate whether PMA-1-GFP participates in septum formation, the cells were stained with the vital dye FM4-64. FM4-64 accumulated at the septum during its formation, when no PMA-1-GFP could be observed (Fig. 4A to C; see also Movie S1 in the supplemental material). FM4-64 was

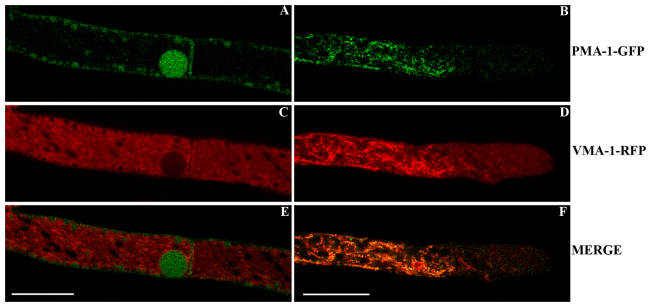

FIG 3 PMA-1-GFP localizes in the lumens of both tubular and spherical vacuoles, whereas VMA-1-RFP is found in the vacuolar membrane. (A and B) PMA-GFP; (C and D) VMA-1-RFP; (E and F) merge. The left column shows the distal region (spherical vacuoles), and the right column shows the apical region (tubular vacuoles). Bar = 20 μm.

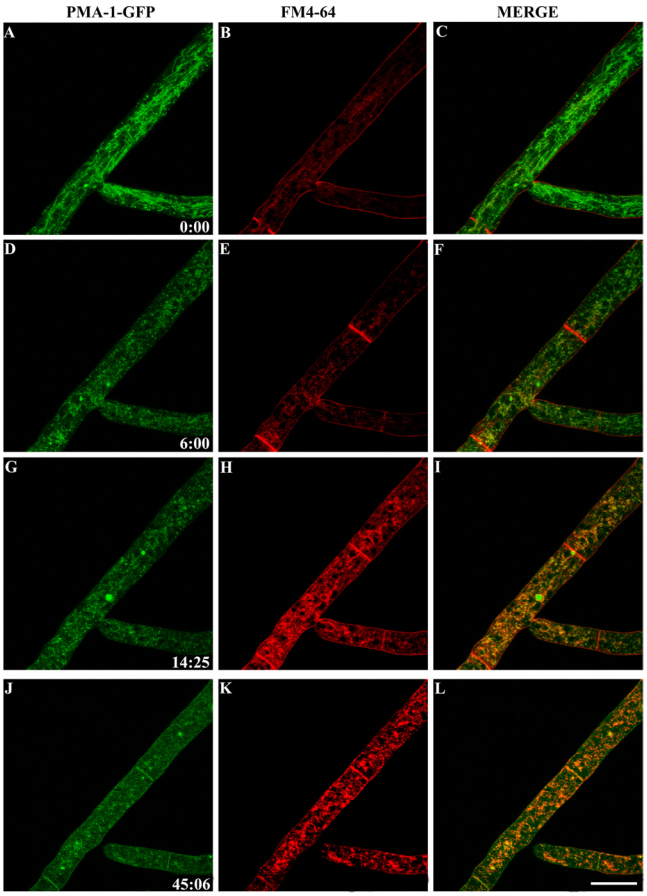

FIG 4 PMA-1-GFP localized at the PM of already-formed septa. (A to C) No GFP fluorescence could be seen at the nascent septa stained with FM4-64 (10 μM). (D to G) After 6 min, septa stained with FM4-64 seemed to be completed, whereas no PMA-1-GFP could be still observed. (G to I) After 14 min 25 s, PMA-1-GFP started to faintly accumulate at completed septa. (J to L) After 45 min 6 s, PMA-1-GFP was clearly observed at completed septa. Bar = 20 μm.

visible at septa after 6 min (Fig. 4E), whereas PMA-1-GFP was not visible at septa until 39 min later (Fig. 4J).

FRAP is a widely used technique to assess the mobility of a fluorescently tagged protein (38, 39). FRAP analysis was conducted to analyze the dynamics of PMA-1-GFP incorporation into the PM and discern whether its delivery occurs from vesicles arriving from the cytoplasm or via lateral diffusion of PMA-1-GFP already incorporated into the lipid bilayer in adjacent regions. After exposure to high-intensity laser irradiation, fluorescence in the PM disappeared and started gradually reappearing until it was almost fully reestablished (Fig. 5). Different photobleaching tests were conducted. First, three small different regions of interest (ROIs) of the PM were selected. This allowed us to analyze FRAP in the photobleached regions and also iFRAP (inverse FRAP) in the unbleached regions contiguous to the photobleached regions (Fig. 5A). Second, a large ROI including the whole span of the PM within a hyphal compartment was selected (Fig. 5B). Finally, an ROI including the cytoplasm contained within a hyphal compartment was selected (Fig. 5C). Fluorescence recovery values were plotted, and variables, such as the mobile fraction (Mf; fraction of fluorescent proteins that diffuse into the bleached region) and the recovery half-time ($t_{1/2}$), were calculated. Low $t_{1/2}$ values (28 to 50 s) were obtained for ROIs including the PM, whereas high $t_{1/2}$ values (550 s) were obtained for ROIs that included the cytoplasm (Fig. 5), indicating that PMA-1-GFP moved from the cytoplasm to the PM. In all cases, the Mf had similar values (81 to 87% [Fig. 5A to C]). iFRAP revealed loss of fluorescence in unbleached regions of the PM (Mf = 45%; $t_{1/2}$ = 49 s [Fig. 5A]), indicating additional lateral diffusion of PMA-1-GFP. Fluorescence in the regions where iFRAP was analyzed did not fully recover, although it gradually reached an intensity that coincided with the fluorescence intensity of adjacent bleached regions (not shown).

PMA-1-GFP is excluded from the Spitzenkörper. Most hypotheses about fungal growth suggest a unidirectional traffic of vesicles to the hyphal apex and a temporary aggregation at the Spitzenkörper, followed by fusion with the apical PM by the process of exocytosis (40). Clearly, PMA-1-GFP did not accumulate in the Spitzenkörper (Fig. 6A and E; see also Movie S1 in the supplemental material). We observed that PMA-1-GFP was incorporated at the PM in distal areas. To rule out the possibility that the presence of a functional Spitzenkörper could conceivably preclude PMA-1 localization at the tip, several cytoskeleton inhibitors shown earlier to disturb Spitzenkörper integrity were used. When either the microtubular or the actin cytoskeleton was disrupted, and no Spitzenkörper was visible, PMA-1-GFP was still localized at the PM and absent at the apex (Fig. 6B to D and G to K). Cytochalasin A and latrunculin A disturbed the FM4-64-stained Spitzenkörper, while benomyl had a less drastic effect but still reduced the Spitzenkörper size and stability, as previously shown (41). PMA-1-GFP was found closer to apical regions of the PM in all cases, presumably because the cytoskeleton inhibitors perturb cell polarization.

In addition, during branch emergence it was observed that the tubular vacuoles are present in the branch but keep a certain distance from the tip. Also, PMA-1-GFP started to localize in the PM of the base of the branch only when it was also localized in the PM of the main hyphae (see Movies S1 and S2 in the supplemental material).

Brefeldin A affects the distribution of PMA-1-GFP. BFA is an inhibitor of the classical ER-Golgi secretory pathway, traditionally used to block vesicle budding from the Golgi. *N. crassa* expressing PMA-1-GFP was exposed to BFA (200 μg/ml) and analyzed by LSCM. After 7 min of exposure, growth ceased and PMA-1-GFP started to accumulate at putative "brefeldin bodies" in subapical and distal regions (Fig. 7A, arrows). After 30 min of exposure, hyphal tips started to swell and small vesicles began to accumulate in apical regions (Fig. 7B). After 90 min, PMA-1-GFP started to accumulate in the PM of apical regions (Fig. 7C). Approximately 2 h later, the tips were swollen, and PMA-1-GFP was distributed throughout the PM all along the hypha, including the apical and subapical regions (Fig. 7D). From that point on, hyphae began to recover and to display polarized growth (data not shown).

To elucidate whether the tubular endomembranes observed in apical regions which become vesicular when exposed to BFA are part of the endosomal pathway, we used FRAP analysis in spherical vacuoles located near the subapical region. Spherical vacuoles near subapical regions were exposed to high-intensity laser irradiation in the presence or absence of BFA. In the absence of BFA (Fig. 8A to D), the fluorescence in the spherical vacuoles started to recover after 5 s (Fig. 8C), and it was fully recovered at 3 min 50 s (Fig. 8D). However, in the presence of BFA (200 μg/ml) (Fig. 8E to

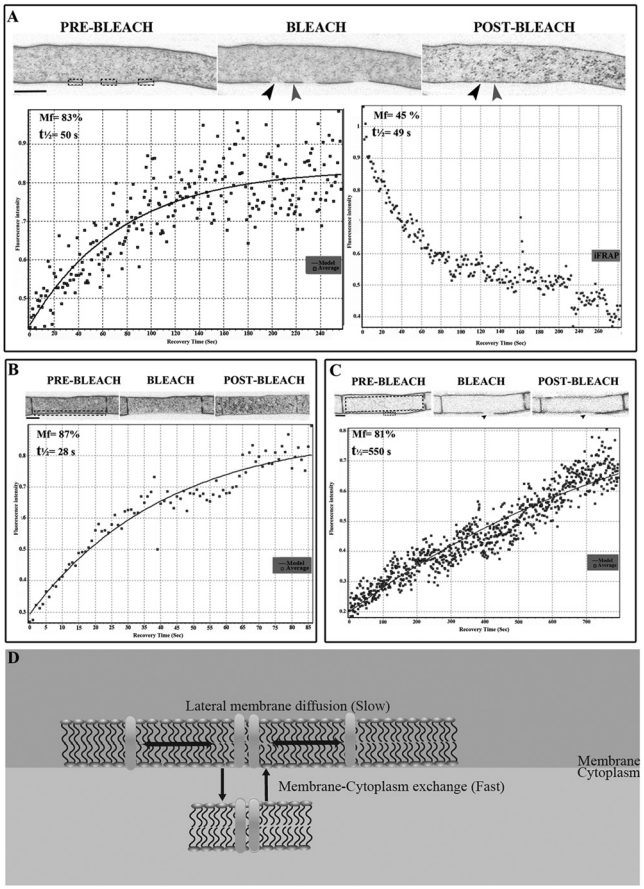

FIG 5 FRAP analysis of PMA-1-GFP fluorescence at the plasma membrane. (A) Three small different ROIs were photobleached (dashed boxes). Black arrowheads indicate photobleached ROIs for which FRAP analysis was conducted, and gray arrowheads show ROIs selected for iFRAP analysis. Bar = 20 μm. (B) A large ROI along the plasma membrane (dashed box) was photobleached. Bar = 10 μm. (C) An ROI including the cytoplasmic region contained within a hyphal compartment and a small ROI in the PM were selected. Black arrowheads indicate ROIs for which FRAP analysis was conducted. Bar = 10 μm. In each case, localization of PMA-1-GFP before and after photobleaching is shown. Graphs show normalized plots of fluorescence recovery values and fitted curves. Mf and $t_{1/2}$ values are shown in each analysis. (D) Scheme showing lateral diffusion of a protein within the PM lipid bilayer versus exchange from an endomembrane to the PM.

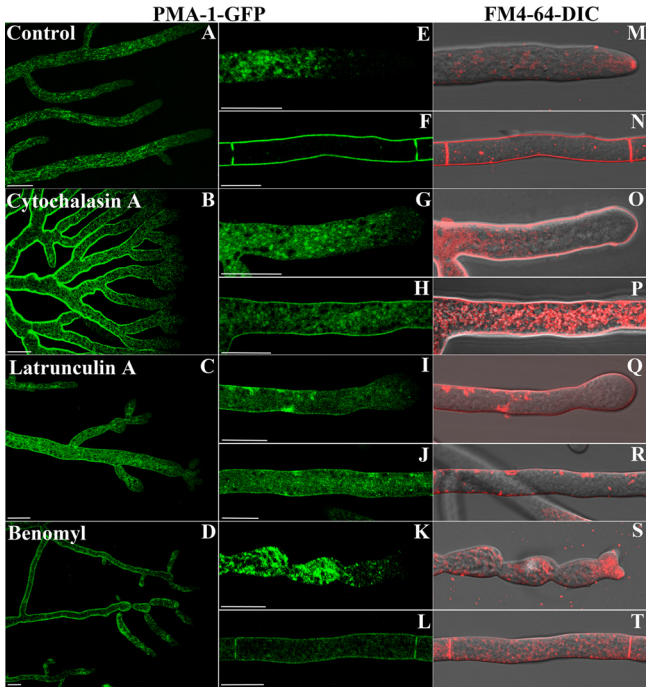

FIG 6 Effects of cytoskeletal inhibitors on PMA-1-GFP localization. (A to D) Hyphae at low magnification; (E to L) PMA-1-GFP fluorescence at high magnification; (M to T) FM4-64 staining. For each treatment, a hyphal tip (top) and a hyphal distal region (bottom) are shown. Untreated cells (A, E, and F) showed PMA-1-GFP fluorescence at tubular endomembranes in subapical regions and at the PM in distal regions. A prominent Spitzenkörper was observed stained by FM4-64 at hyphal apices. Hyphae treated with cytochalasin A showed initial swelling of tips followed by dichotomous branching (B, G, and O) and abnormal PMA-1-GFP distribution (B, G, and H); fluorescence could no longer be observed in tubular endomembranes, and at the PM, it extended toward subapical regions (B and G). No Spitzenkörper was present at the tips (O). Hyphae treated with latrunculin A displayed swollen tips (C, I, and Q). PMA-1-GFP was observed at the PM near subabipal regions (C and I), and no Spitzenkörper was present at the apices (Q). In addition, PMA-1-GFP and FM 4-64 colocalized fluorescence could be observed accumulating cortically, below the cell surface in subapical and distal regions, indicative of impaired endocytosis (I, J, Q, and R). Hyphae treated with benomyl showed distorted morphology (D). PMA-1-GFP fluorescence at the subapical tubular endomembranes was more prominent (K), and at the PM, it extended toward subapical regions (D). The Spitzenkörper appeared reduced in size and integrity (S). In all cases, PMA-1-GFP continued to be localized in the PM in distal regions (F, H, J, and L). Cytochalasin A was used at 100 μg/ml, latrunculin A at 20 μg/ml, and benomyl at 50 μg/ml. Bars = 10 μm (A to D) and 20 μm (E to T).

H), fluorescence at vacuoles was not recovered after 4 min 30 s (Fig. 8H).

DISCUSSION

PMA-1 is excluded from the apical region. Traffic of PMA-1-GFP provides insight into one of the pathways that delivers proteins from the Golgi to the cell surface in fungal hyphae.

Our studies demonstrate that H^+-ATPase is differentially distributed along the fungal cell surface in mature hyphae. PMA-1-GFP was found at the cell surface of subapical and distal parts but not at the apex. These results confirm earlier predictions that the H^+-ATPase is deficient or inactive at the apex but abundant distally (9). Protons are expelled distally by the proton-translocating ATPase and enter the apical region by a number of transporters, including those carrying potassium and phosphate ions as previously reported (9). Furthermore, the distribution of PMA-1-GFP in the PM is in agreement with the intracellular pH gradient in *N. crassa*. Analysis of intracellular pH using bromocresol green (a pH indicator) showed that apical zones, devoid of PMA-1, have an acid pH, whereas distal regions, in which PMA-1 is abundant, have a basic pH (8). A similar cytochemical gradient was observed in other filamentous fungi (6).

Some proteins, such as transporter or symporter proteins, need protons for their function, suggesting that these proteins may use the electrochemical gradient created by the H^+-ATPase. In *S. cerevisiae*, the arginine/H^+ transporter Can1p, like Pma1p, is also found in all regions of the PM (42). However, Pma1p and Can1p occupy different PM microdomains, which confirmed the existence of protein compartmentation within the PM in yeast (42). Protein compartmentation probably also exists within the PM of *N. crassa*. In, *N. crassa* the basic amino acid permease PMB, the homolog of Can1p, tagged with GFP displayed a distribution sim-

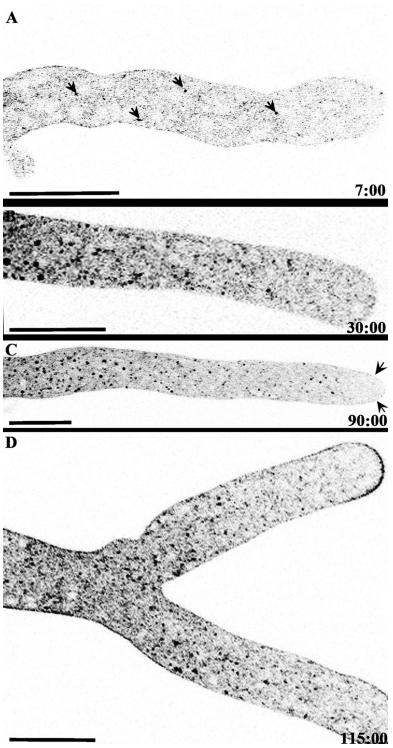

FIG 7 Effects of brefeldin A (200 μg/ml) on *N. crassa* mature hyphae expressing PMA-1-GFP. (A) After 7 min of exposure, PMA-1-GFP began to accumulate at putative brefeldin bodies (arrows in subapical and distal regions). (B and C) After 30 to 90 min of exposure, the tip began to swell and PMA-1-GFP started to accumulate at the PM of the apex. (D) After 2 h of exposure, PMA-1-GFP accumulated throughout the PM all along the hypha, including the apex and subapex. Bars = 20 μm.

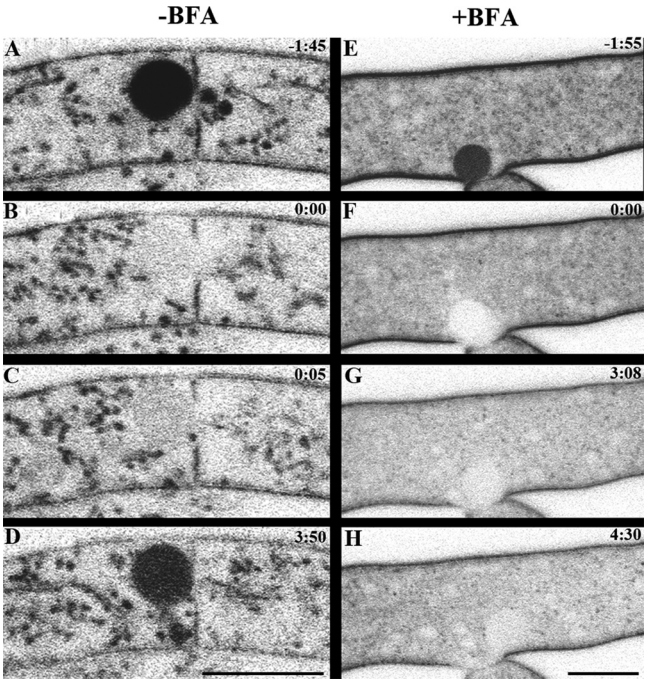

FIG 8 FRAP analysis in spherical vacuoles near the subapical regions of *N. crassa* hyphae treated with BFA (200 μg/ml). (A to D) FRAP in untreated hyphae; (E to H) FRAP in hyphae exposed to BFA. (A and E) Fluorescence in a spherical vacuole before photobleaching; (B and F) photobleaching of fluorescence in a spherical vacuole; (C) fluorescence recovery in a spherical vacuole of an untreated hypha 5 s after photobleaching; (D) fluorescence recovered completely after 3 min 50 s; (G and H) fluorescence of a spherical vacuole in a hypha exposed to BFA did not recover after 4 min 30 s. Bars = 20 μm.

ilar to that of PMA-1 (see Fig. S5 in the supplemental material). Coexpression of PMA-1 and PMB tagged with different fluorescent markers and a higher-resolution microscopic analysis are needed to discern whether these two proteins occupy different PM microdomains in the range of several hundred nanometers.

Exocytosis occurs in distal regions of hyphae. Even though PMA-1-GFP was found in cell fractions of a density corresponding to that of ER and macrovesicles (35), it did not accumulate at the Spitzenkörper, where there is the highest concentration of secretory vesicles according to electron micrographs of hyphal tips of *N. crassa* (36). Instead, PMA-1-GFP localizes in subapical regions and is somehow directly delivered to the PM.

FRAP analysis revealed rates of fluorescence recovery higher for cytoplasmic exchange than for lateral diffusion, suggesting that PMA-1 is incorporated to the PM primarily by membrane-cytoplasmic exchange. However, lateral diffusion also occurs, as could be inferred from the iFRAP results. FRAP analysis suggests continuous exocytosis of PMA-1 to the PM in distal regions. Some SNARE proteins and components of the exocyst complex (AoSec3) which are involved in exocytosis events have been localized in the septum and PM in *Aspergillus oryzae* (43, 44). In *A. oryzae*, it has been shown that transport proteins are expressed primarily in distal regions. For instance, AoUapC and AoGap1, two amino acid permeases, did not accumulate at the Spitzenkörper. They were observed in lateral PM and septa (43, 45). Some mechanisms of exocytosis, such as kiss-and-run (K&R) mechanisms, do not involve growth of the PM (46–48). During K&R, proteins are released but the vesicles do not fully collapse; i.e., the vesicle membrane does not fuse completely with the PM and does not contribute to membrane expansion (49). While K&R mechanisms have not been explored or identified in yeast or filamentous fungi, the collective evidence suggests that they may exist. Intuitively, in growing hyphae, if all the vesicular membrane exocytosed at areas other than the tip contributed to an increase in the hyphal surface area, endocytosis would have to occur at regions of the hyphae other than the subapical collar suggested by several authors (50–53). Clearly, future studies are needed to quantitatively analyze the contribution of each of these processes to cell growth.

PMA-1 recycling involves the endosomal pathway. After a short exposure to BFA, PMA-1-GFP delivery to the PM was not apparently blocked in *N. crassa* hyphae. In addition, PMA-1-GFP accumulated at small structures visible in apical and subapical regions, similarly to the brefeldin bodies or "brefeldin organelles" observed in *Aspergillus nidulans* and *S. cerevisiae* cells expressing fluorescently labeled Golgi markers PH^{OSBP}, HypB^{Sec7}, and Sec7p, respectively, when exposed to BFA (54–56). As mentioned earlier, Pma1p is very stable in the PM; therefore, the fact that we still see it in the PM after short exposure to BFA could indicate that even if no additional PMA-1-GFP arrives at the PM, the protein existing at the time the drug was applied has not been yet recycled. Upon longer exposure to BFA, PMA-1-GFP was found at the PM in apical regions, indicating that somehow the apex lost its "polar" markers and PMA-1 was missorted to all regions of the PM. What

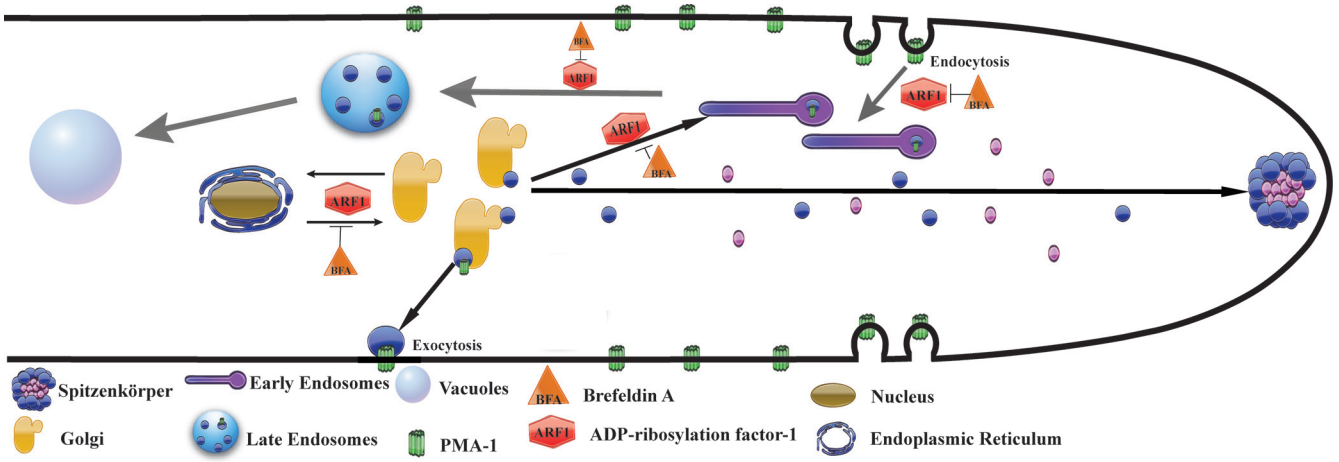

FIG 9 PMA-1 secretion and recycling model. This model proposes a classical secretory ER-to-Golgi pathway of PMA-1 that finally gets incorporated into the PM (black arrows), while recycling would occur via the endosomal pathway (gray arrows). Under normal growth conditions, PMA-1 is found in tubular endomembranes in apical regions and vacuoles in the distal regions. The main target of BFA is Sec7, a Golgi-localized Arf1 guanine exchange factor. Treatment with BFA acts on Sec7 (in domains necessary to activate Arf1, which remains locked in the GDP-bound inactive conformation), blocks the route of budding vesicles from the ER to the Golgi, and also blocks the endosome recycling pathway. Consequently, PMA-1 does not accumulate at spherical vacuoles and appears at what would correspond to brefeldin bodies (not shown).

could not be discerned at this stage is whether PMA-1-GFP would arrive at the apical PM by lateral diffusion of protein from more distal areas, given that no new PMA-1-GFP presumably traffics from the Golgi to the PM. In addition, it has been suggested that BFA enhances a secondary pathway (57). BFA has an additional site of action beyond the Golgi, one that affects endosomes (58). We observed that PMA-1-GFP was not arriving at spherical vacuoles, and tubular endomembranes disappeared when hyphae were treated with BFA. The function of the tubular endomembrane compartment is unclear. In addition to PMA-1 and VMA-1 (a subunit of the vacuolar ATPase), the same tubules have been shown to contain two Ca^{2+}-ATPases (NCA-2 and NCA-3) that also localize to the PM and a calcium-proton exchange protein (CAX) that localizes to the vacuoles (59). This suggests an endosomal sorting function for these tubular organelles (Fig. 9). Transport between early endosomes (EE) and late endosomes (LE) involves an Arf1-dependent recruitment of a subset of COPI vesicle coat polypeptides. In *S. cerevisiae* and mammalian cells, Arf1 mutants exhibit similar defects in endocytosis and the secretory pathway (60). In addition, it has been shown that Vps (vacuolar protein sorting) proteins participate in the trafficking of a Pma1p from the Golgi to the PM via the endosome pathway (61).

Final remarks. This work suggests the presence of a targeting mechanism independent of the Spitzenkörper that ensures delivery of essential proteins, such as PMA-1, to the PM in nongrowing regions of the hyphae. These results open up new questions about secretion in filamentous fungi. It remains to be studied how PMA-1 gets incorporated at the PM and whether there exists a K&R mechanism or other types of alternative exocytosis mechanisms in filamentous fungi.

ACKNOWLEDGMENTS

We are grateful to Michael Freitag (Oregon State University) for his valuable contributions to this work. We also thank Eddy Sánchez (CICESE) for generous technical assistance.

This work was initially supported by a UC-MEXUS CONACyT Collaborative Research Grant to M.R. and B.B. We acknowledge CONACYT grant B0C022 to M.R. and a CONACYT fellowship to R.A.F.-S., which allowed completion of this study.

REFERENCES

1. **Bartnicki-García S, Hergert F, Gierz J.** 1989. Computer simulation of fungal morphogenesis and the mathematical basis for hyphal tip growth. Protoplasma **153:**46–57.
2. **Slayman CL.** 1987. The plasma membrane ATPase of *Neurospora*: a proton-pumping electroenzyme. J. Bioenerg. Biomembr. **19:**1–20.
3. **Potapova TV, Aslanidi KB, Belozerskaya TA, Levina NN.** 1988. Transcellular ionic currents studied by intracellular potential recordings in *Neurospora crassa* hyphae. Transfer of energy from proximal to apical cells. FEBS Lett. **241:**173–176.
4. **Belozerskaya TA, Potapova TV.** 1993. Intrahyphal communication in segmented mycelium. Exp. Mycol. **17:**157–169.
5. **Nakamoto RK, Rao R, Slayman CW.** 1991. Expression of the yeast plasma membrane [H^+] ATPase in secretory vesicles. A new strategy for directed mutagenesis. J. Biol. Chem. **266:**7940–7949.
6. **Turian G.** 1979. Cytochemical gradients and mitochondrial exclusion in the apices of vegetative hyphae. Experientia **37:**1164–1166.
7. **Gow N.** 1984. Transhyphal electrical currents in fungi. J. Gen. Microbiol. **130:**3313–3318.
8. **McGillviray AM, Gow N.** 1987. The transhyphal electrical current of *Neurospora crassa* is carried principally by protons. J. Gen. Microbiol. **133:**2875–2881.
9. **Takeuchi G, Shmidt J, Caldwell JH, Harold FM.** 1988. Transcellular ion currents and extension of *Neurospora crassa*. J. Membr. Biol. **101:**33–41.
10. **Serrano R, Kielland-Brandt MC, Fink GR.** 1986. Yeast plasma membrane ATPase is essential for growth and has homology with ($Na^+ + K^+$)-, K^+- and Ca^{2+}-ATPases. Nature **319:**689–693.
11. **Hager K.** 1986. Amino acid sequence of the plasma membrane ATPase of *Neurospora crassa*: deduction from genomic and cDNA sequences. Proc. Natl. Acad. Sci. U. S. A. **83:**7693–7697.
12. **Addison R.** 1986. Primary structure of the *Neurospora crassa* plasma membrane H^+-ATPase deduced from the gene sequence. J. Biol. Chem. **261:**14896–14901.
13. **Serrano R.** 1991. Transport across yeast vacuolar and plasma membrane, p 523–585.]?>*In* JonesEW, Broach JR (ed), The molecular and cellular biology of the yeast Saccharomyces: genome dynamics, protein synthesis, and energetics. Cold Spring Harbor Laboratory Press, Cold Spring Harbor, NY.
14. **Bowman BJ, Blasco F, Slayman CW.** 1981. Purification and characterization of the plasma membrane ATPase of *Neurospora crassa*. J. Biol. Chem. **256:**12343–12349.

15. **Brada D, Schekman R.** 1988. Coincident localization of secretory and plasma membrane proteins in organelles of the yeast secretory pathway. J. Bacteriol. **170:**2775–2783.
16. **Holcomb CL, Hansen WJ, Etcheverry T, Shekman R.** 1988. Secretory vesicles externalize the major plasma membrane ATPase in yeast. J. Cell Biol. **106:**641–648.
17. **Chang A, Slayman CW.** 1991. Maturation of the yeast plasma membrane [H^+] ATPase involves phosphorylation during intracellular transport. J. Cell Biol. **115:**289–295.
18. **Roberg KJ, Crotwell M, Espenshade P, Gimeno R, Kaiser CA.** 1999. LST1 is a SEC24 homologue used for selective export of the plasma membrane ATPase from the endoplasmic reticulum. J. Cell Biol. **145:**659–672.
19. **Shimoni Y, Kurihara T, Ravazzola M, Amherdt M, Orci L, Schekman R.** 2000. Lst1p and Sec24p cooperate in sorting of the plasma membrane ATPase into COPII vesicles in *Saccharomyces cerevisiae*. J. Cell Biol. **151:**973–984.
20. **Chang A, Fink GR.** 1995. Targeting of the yeast plasma membrane [H^+] ATPase: a novel gene *AST*1 prevents mislocalization of mutant ATPase to the vacuole. J. Cell Biol. **128:**39–49.
21. **Benito B, Moreno E, Lagunas R.** 1991. Half-life of the plasma membrane ATPase and its activating system in resting yeast cells. Biochim. Biophys. Acta **1063:**265–268.
22. **Stack JH, Horazdovsky B, Emr SD.** 1995. Receptor-mediated protein sorting to the vacuole in yeast: roles for a protein kinase, a lipid kinase and GTP-binding proteins. Annu. Rev. Cell Dev. Biol. **11:**1–33.
23. **Bagnat M, Chang A, Simons K.** 2001. Plasma membrane proton ATPase Pma1p requires raft association for surface delivery in yeast. Mol. Biol. Cell **12:**4129–4138.
24. **Eisenkolb M, Zenzmaier C, Leitner E, Schneiter R.** 2002. A specific structural requirements for ergosterol in long-chain fatty acid synthesis mutants important for maintaining raft domains in yeast. Mol. Biol. Cell **13:**4414–4428.
25. **Vogel HJ.** 1956. A convenient growth medium for *Neurospora* (medium N). Microbiol. Gen. Bull. **13:**42–43.
26. Reference deleted.
27. **Hickey PC, Jacobson D, Read ND, Glass NL.** 2002. Live-cell imaging of vegetative hyphal fusion in *Neurospora crassa*. Fungal Genet. Biol. **37:**109–119.
28. **Sambrook J, Fritsch EF, Maniatis T.** 1989. Molecular cloning: a laboratory manual, 2nd ed. Cold Spring Harbor Laboratory Press, Cold Spring Harbor, NY.
29. **Freitag M, Hickey PC, Raju NB, Selker EU, Read ND.** 2004. GFP as a tool to analyze the organization, dynamics and function of nuclei and microtubules in *Neurospora crassa*. Fungal Genet. Biol. **41:**897–910.
30. **Honda S, Selker EU.** 2009. Tools for fungal proteomics: multifunctional Neurospora vectors for gene replacement, protein expression and protein purification. Genetics **1:**11–23.
31. **Riquelme M, Bartnicki-García S, González-Prieto JM, Sánchez-León E, Verdín-Ramos J, Beltrán-Aguilar A, Freitag M.** 2007. Spitzenkörper localization and intracellular traffic of green fluorescent protein-labeled CHS-3 and CHS-6 chitin synthases in living hyphae of *Neurospora crassa*. Eukaryot. Cell **6:**1853–1864.
32. **Shiu PK, Zickler D, Raju NB, Ruprich-Robert G, Metzenberg RL.** 2006. SAD-2 is required for meiotic silencing by unpaired DNA and perinuclear localization of SAD-1 RNA-directed RNA polymerase. Proc. Natl. Acad. Sci. U. S. A. **103:**2243–2248.
33. **Richthammer C, Enseleit M, Sanchez-Leon E, März S, Heilig Y, Riquelme M, Seiler S.** 2012. RHO1 and RHO2 share partially overlapping functions in the regulation of cell wall integrity and hyphal polarity in *Neurospora crassa*. Mol. Microbiol. **85:**716–733.
34. **Leal-Morales CA, Bracker CE, Bartnicki-García S.** 1994. Subcellular localization, abundance and stability of chitin synthetases 1 and 2 from *Saccharomyces cerevisiae*. Microbiology **140:**2207–2216.
35. **Verdín J, Bartnicki-García S, Riquelme M.** 2009. Functional stratification of the Spitzenkörper of *Neurospora crassa*. Mol. Microbiol. **74:**1044–1053.
36. **Riquelme M, Roberson RW, McDaniel DP, Bartnicki-Garcia S.** 2002. The effects of *ropy-1* mutation on cytoplasmic organization and intracellular motility in mature hyphae of *Neurospora crassa*. Fungal Genet. Biol. **37:**171–179.
37. **Araujo-Palomares CL, Castro-Longoria E, Riquelme M.** 2007. Ontogeny of the Spitzenkörper in germlings of *Neurospora crassa*. Fungal Genet. Biol. **44:**492–503.
38. **Lippincott-Schwartz J, Snapp E, Kenworthy A.** 2001. Studying protein dynamics in living cells. Nat. Rev. Mol. Cell Biol. **2:**444–456.
39. **Goehring NW, Chowdhury D, Hyman AA, Grill SW.** 2010. FRAP analysis of membrane-associated proteins: lateral diffusion and membrane-cytoplasmic exchange. Biophys. J. **99:**2443–2452.
40. **Bartnicki-García S.** 2006. Chitosomes: past, present and future. FEMS Yeast Res. **6:**957–965.
41. **Riquelme M, Gierz G, Bartnicki-García S.** 2000. Dynein and dynactin deficiencies affect the formation and function of the Spitzenköper and distort hyphal morphogenesis of *Neurospora crassa*. Microbiology **146:**1743–1752.
42. **Malínská K, Malínský J, Opekarová M, Tanner W.** 2003. Visualization of protein compartmentation within the plasma membrane of living yeast cells. Mol. Biol. Cell **11:**4427–4436.
43. **Hayakawa Y, Ishikawa E, Shoji JY, Nakano H, Kitamoto K.** 2011. Septum-directed secretion in the filamentous fungus *Aspergillus oryzae*. Mol. Microbiol. **1:**40–55.
44. **Kuratsu M, Taura A, Shoji JY, Kikuchi S, Arioka M, Kitamoto K.** 2007. Systematic analysis of SNARE localization in the filamentous fungus *Aspergillus oryzae*. Fungal Genet. Biol. **44:**1310–1323.
45. **Masai K, Maruyama J, Sakamoto K, Nakajima H, Akita O, Kitamoto K.** 2006. Square-plate culture method allows detection of differential gene expression and screening of novel, region-specific genes in *Aspergillus oryzae*. Appl. Microbiol. Biotechnol. **71:**881–891.
46. **Alés E, Tabares L, Poyato JM, Valero V, Lindau M, Alvarez de Toledo G.** 1999. High calcium concentrations shift the mode of exocytosis to the kiss-and-run mechanism. Nat. Cell Biol. **1:**40–44.
47. **Henkel AW, Meiri H, Horstmann H, Lindau M, Almers W.** 2000. Rhythmic opening and closing of vesicles during constitutive exo- and endocytosis in chromaffin cells. EMBO J. **19:**84–93.
48. **Lollike K, Borregaard N, Lindau M.** 1998. Capacitance flickers and pseudoflickers of small granules, measured in the cell-attached configuration. Biophys. J. **75:**53–59.
49. **Keighron J, Ewing AG, Cans AS.** 2012. Analytical tools to monitor exocytosis: a focus on new fluorescent probes and methods. Analyst **137:**1755–1763.
50. **Delgado-Álvarez DL, Callejas-Negrete OA, Gómez N, Freitag M, Roberson RW, Smith LG, Mouriño-Pérez RR.** 2010. Visualization of F-actin localization and dynamics with live cell markers in *Neurospora crassa*. Fungal Genet. Biol. **47:**573–586.
51. **Upadhyay S, Shaw BD.** 2008. The role of actin, fimbrin, and endocytosis in growth of hyphae in *Aspergillus nidulans*. Mol. Microbiol. **68:**690–705.
52. **Araujo-Bazán L, Peñalva MA, Espeso EA.** 2008. Preferential localization of the endocytic internalization machinery to hyphal tips underlies polarization of the actin cytoskeleton in Aspergillus nidulans. Mol. Microbiol. **67:**891–905.
53. **Taheri-Talesh N, Horio T, Araujo-Bazán L, Dou X, Espeso EA, Peñalva MA, Osmani SA, Oakley BR.** 2008. The tip growth apparatus of Aspergillus nidulans. Mol. Biol. Cell **19:**1439–1449.
54. **Pantazopoulou A, Peñalva MA.** 2009. Organization and dynamics of the *Aspergillus nidulans* Golgi during apical extension and mitosis. Mol. Biol. Cell **20:**4335–4347.
55. **Rambourg A, Clermont Y, Jackson CL, Kepes F.** 1995. Effects of brefeldin A on the three-dimensional structure of the Golgi apparatus in a sensitive strain of *Saccharomyces cerevisiae*. Anat. Rec. **241:**1–9.
56. **Deitz SB, Rambourg A, Kepes F, Franzusoff A.** 2000. Sec7p directs the transitions required for yeast Golgi biogenesis. Traffic **1:**172–183.
57. **Klausner RD, Donaldson JG, Lippincot-Schwartz J.** 1992. Brefeldin A: insights into the control of membrane traffic and organelle structure. J. Cell Biol. **116:**1071–1080.
58. **Nebenführ A, Ritzenthaler C, Robinson DG.** 2002. Brefeldin A: deciphering an enigmatic inhibitor of secretion. Plant Physiol. **3:**1102–1108.
59. **Bowman BJ, Draskovic M, Freitag M, Bowman EJ.** 2009. Structure and distribution of organelles and cellular location of calcium transporters in *Neurospora crassa*. Eukaryot. Cell **8:**1845–1855.
60. **Gaynor EC, Chen CY, Emr SD, Graham TR.** 1998. ARF is required for maintenance of yeast Golgi and endosome structure and function. Mol. Biol. Cell **9:**653–670.
61. **Luo W, Chang A.** 2000. An endosome-to-plasma membrane pathway involved in trafficking of a mutant plasma membrane ATPase in yeast. Mol. Biol. Cell **11:**579–592.